RSC Advances

ROYAL SOCIETY OF CHEMISTRY

www.rsc.org/advances

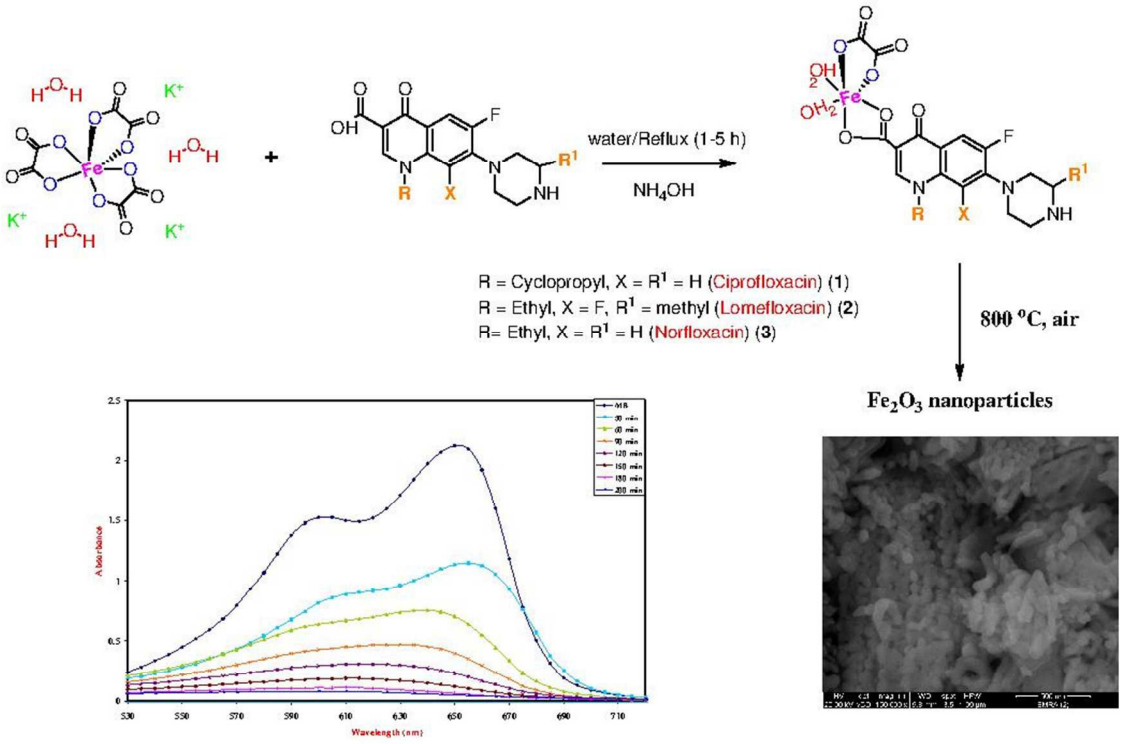

Photocatalytic degradation of methylene blue with hematite nanoparticles synthesized by thermal decomposition of fluoroquinolones oxalato-iron(III) complexes

Ahmed M. Mansour*

Chemistry Department, Faculty of Science, Cairo University, Gamaa Street, Giza 12613, Egypt

Abstract

$[Fe(C_2O_4)(FQ)(H_2O)_2]$ complexes (H-FQ = ciprofloxacin (**1**), lomefloxacin (**2**) and norfloxacin (**3**)) were synthesized and characterized using a variety of analytical and spectral techniques such as elemental analysis, infrared spectroscopy, thermogravimetric analysis, ultraviolet-visible spectroscopy, magnetic and conductance measurements. The experimental studies were complemented by quantum chemical calculations in terms of geometry optimization, natural bond orbital analysis and molecular electrostatic potential maps. Electronic structures were discussed by TD-DFT. Hematite (α-Fe_2O_3) nanoparticles, as a promising material for different catalytic applications, were prepared in air *via* the controlled thermal decomposition of **1-3**. Powder X-ray diffraction was used to identify the polymorph of iron oxide. The morphology of nano-hematite was investigated by a field emission scanning electron microscope coupled to energy-dispersive X-ray spectroscopy for surface analysis. The catalytic degrad--ation of methylene-blue (MB), as industrial pollutant, exposed to UV radiation in presence of nano-α-Fe_2O_3 as a catalyst and hydrogen peroxide as the oxidant was studied at room temperature in water.

Key Words: Fluoroquinolones; Oxalato complexes; NBO; Catalytic activity; Methylene-blue

* Corresponding author, Tel.: +2 02 01222211253; Fax: +20 2 35728843. E-mail: inorganic_am@ yahoo.com; mansour@sci.cu.edu.eg

Introduction

So far, the oxalato ligand has appeared as a fertile key for design complexes of intriguing structural research applications **[1]**. Normally, the oxalato can act as a chelating or bridging ligand **[2,3]** . The $[M^{III}(C_2O_4)_3]^{3-}$ complexes of Al and transition metal ions have been extensively studied **[4-16]**. In 1939 **[5]**, Blair and Jones synthesized potassium tris(oxalato)ferrate(III) trihydrate (KOF) from FeC_2O_4. Recently, a modified synthesis method has been introduced by Hussain *et al.* **[6]** through the reaction of a mixture of $K_2C_2O_4 \cdot H_2O$ and $H_2C_2O_4 \cdot 2H_2O$ with $Fe(OH)_3$. Crystal structures of anhydrous **[6]** and hydrated forms **[7]** of KOF showed the existence of an infinite anionic distorted octahedral $[Fe(C_2O_4)_3]^{3-}$ units and the three K^+ ions are coordinated by water or oxalato ligands. The importance of KOF is ascribed to being a chemical actinometer. This complex undergoes a color change when it is heated **[8]** or if the aqueous solution is exposed to UV radiation **[9]** suggesting the reduction of Fe^{3+} and formation of ion-radical intermediate, $C_2O_4^{\cdot-}$ **[10,11]**. The photo-chemical significance of KOF has been extended to the field of polymer chemistry e.g. the photo-polymerization of acrylamide **[12]** and methyl methacrylate **[13]** in the aqueous acid solution of KOF has been achieved. Another application of KOF has been gained from the preparation of nano-Fe_2O_3 *via* the solid state thermolysis process **[14]**. Different polymorphs nanoparticles were obtained at the different temperatures **[8, 15, 16]** .

Fluoroquinolones (FQ's) represent a group of synthetic antibiotics distinguished by a good bioavailability, safety profile, long half-life (with once-daily dosing) and a broad antibacterial spectrum against gram(-) bacteria **[17, 18]**. Ciprofloxacin (H-Cf) (Scheme 1) is a second-generation quinolone drug used for the treatment of urinary zone infections, bone and joint infections, infectious diarrhea, typhoid fever and acute sinusitis **[19]**. Norfloxacin (H-Nf) is the first FQ drug introduced to the market. Its antibacterial activity of H-Nf involves multi-antibiotic resistant, gram(-) rods and beta-lactamase producing organisms. Lomefloxacin (H-Lf) is a third-generation quinolone used in cure of respiratory and urinary tracts, gynecological, ophthalmological and soft tissue infections. It has the advantage of being effective against some anaerobic bacteria **[20]**.

The formation of FQ's complexes with transition and non-transition metal ions was the question of a number of literature reports **[21]**. Several studies **[22-31]** concerning the interactions between H-Cf, H-Lf and H-Nf and Fe^{3+} ions were reported. A simple rapid spectral method was developed for determination of H-Cf in its pharmaceutical formulations using $Fe(NO_3)_3$ **[22]**. Formation constants of Fe^{3+} complexes of H-Cf and H-Nf were determined **[23]**. The water-soluble $Fe(Nf)_2^+$ (λ_{max} = 377 nm) formed in the acidic medium was used for determination of Fe^{3+} **[24]**. The complexation of H-Lf with

Fe^{3+} ions in terms of stability constants and stoichiometries was studied by Riley *et al.* **[25]**. Complexes of the type $[Fe(Nf)_2(H_2O)_2]Cl_3 \cdot 6H_2O$ **[26]**, $[Fe(Nf)_3]Cl_3 \cdot 12H_2O$ **[27]**, [Fe(Cf)(nitrilotriacetate)]·$3.5H_2O$ **[28]**, $[Fe(Cf)_3]$ **[29]** and $[Fe(Lf)(H_2O)_4]Cl_3 \cdot H_2O$ **[30]** were proposed, where FQ's interact with Fe^{3+} *via* the carboxylate and pyridione oxygen atoms. Hydrothermal reaction of H-Cf with $Fe(OH)_3$ in presence of oxalate yields $[Fe(H\text{-}Cf)(C_2O_4)_2] \cdot H_2Cf \cdot 5H_2O$ **[31]**.

In the present study, synthesis, spectroscopic and thermal characterization of three mononuclear iron(III)-oxalato complexes containing fluoroquinolones (ciprofloxacin, lomefloxacin and norfloxacin) as a secondary ligand (Scheme 1) are reported both experimentally and theoretically. Due to the wide variety of applications for iron oxide nanoparticle polymorphs in the fields of catalysis **[32]**, sensors **[33]**, clinical diagnosis **[34]**, and magnetic storage **[35]**, a simple and nontoxic method for preparation of α-Fe_2O_3 nanoparticles based upon the thermal decomposition of $[Fe(C_2O_4)(FQ)(H_2O)_2]$ complexes has been explored. The morphology has been characterized by different physical methods such as XRD , and FE-SEM. The surface analysis has been carried out by EDX. Finally, the degradation of MB by Fenton-like catalytic performance of α-Fe_2O_3 nanoparticles has been investigated with the aid of the ultraviolet radiation.

Results and discussion

Spectral and magnetic characterization

The reaction of KOF with one equivalent of FQ's (Scheme 1) affords complexes of the type $[Fe(C_2O_4)(FQ)(H_2O)_2]$ (H-FQ = H-Cf (**1**), H-Lf (**2**) and H-Nf (**3**)). These complexes were characterized by elemental analysis, TGA, IR, UV-vis., magnetic and molar conductance measurements. The active IR bands at 1707, 1624 cm^{-1} (H-Cf·HCl), 1723, 1620 cm^{-1} (H-Lf·HCl) and 1708, 1620 cm^{-1} (H-Nf) (Fig. S1†) are assigned to $\nu(COOH)^{carb}$ and $\nu(C=O)^{py}$ (carb: carboxyl, py: pyridone). In complexes, the vanishing of $\nu(COOH)^{carb}$ mode might be a sign for the ionization of -COOH and consequently its involvement in chelation **[36]**. In general, the carboxylate ion gives rise to two bands: a strong asymmetric stretching band near 1650-1550 cm^{-1} and a weaker symmetrical stretching one near 1400 cm^{-1} **[37]**. For example, complex **2** shows the $\nu^{ass}(C \cdots O)$ and $\nu^{ss}(C \cdots O)$ modes at 1554 and 1360 cm^{-1} **[38]** with $\Delta\nu \approx 200$ cm^{-1} characteristic of unidentate COO^- group **[39],** while complex **3** displays only the asymmetric vibration at 1548 cm^{-1}. These modes are overlapped in **1**. The pyridone C=O group is liberated from the intra-molecular H-bond interaction *via* the complex formation and interacts with metal ion giving a band at the higher wave numbers; 1628 (**1**), 1630 (**2**) and 1627 (**3**) **[40]**. In contrast, the piperazine NH is not involved in chelation, since its stretching mode is located at higher wave

numbers **[41]**, 3436-3442 cm^{-1} (**1-3**) compared with 3429-3436 cm^{-1} observed in the free ligands. The weak/medium intensity bands at 1714, 1668 and 1476 cm^{-1} (**1**), 1714, 1670 and 1459 cm^{-1} (**2**), 1713, 1665 and 1477 cm^{-1} (**3**) (Fig. S2†) allocated for $\nu(C{=}O)_{ox}$, $\nu^{ass}(C{=}O)_{ox}$ and $\nu^{ss}(C{=}O)_{ox}$ (ox: oxalato) are taken as evidence for the bidentate nature of the oxalato ligand in the mononuclear complexes **[3, 42]**.

The electronic absorption spectra (Fig. S3†) of **1-3** in DMSO exhibit the intra-ligand transitions at 335, 320 and 285 nm (**1**), 340, 325 and 292 nm (**2**), 335, 320 and 285 nm (**3**) **[38]**. An additional weak band at about 625 nm assigned to $^6A_{1g} \rightarrow {}^5T_{1g}$ transition in a distorted octahedral stereochemistry is observed in the studied complexes **[29]**. The effective magnetic moment values at 298 K, calculated by the spin-only terms, are 4.86, 6.19 and 6.14 μ_B for complexes **1-3** that are in agreement with those expected for high spin arrangement Fe(III) complexes (S = 5/2; μ_{eff} = 5.0-6.1 μ_B) **[43]**.

DFT/TD-DFT

To obtain an insight into the geometrical and electronic structures of the investigated complexes, cis-[$Fe(C_2O_4)(FQ)(H_2O)_2$] were optimized (Fig. 1) by DFT/B3LYP method combined with 6-31G(d). It was found that the cis-isomer is more stable than the trans-isomer by 18.543 KJ/mol. The complexes were characterized as local minima through harmonic frequency analysis. The Fe^{3+} ion displays a distorted FeO_6 octahedral geometry. Four oxygen atoms coming from the chelating oxalato [FeO2 = 1.840 Å and FeO7 ≈ 1.882 Å] and bidentate FQ drug [FeO3 ≈ 1.893 Å and FeO4 ≈ 1.877 Å] are coordinated to the metal ion. The octahedral geometry is completed by two water molecules [FeO5 = 2.033 Å and FeO6 = 2.026 Å] lying in a cis-position. The Fe^{3+}-oxalato bonds are not equal, since the oxalato oxygen atoms are participated in two H-bonds of different strengths [O2...H54-O6 (2.403 Å, < 95.5 º) and O7...H51-O5 (2.094 Å, < 107.3 º)]. As shown in Fig. 1, another two H-bonds affecting the regularity of the geometry [O4...H53-O6 (1.989 Å, < 110.0 º) and O6...H52-O5 (2.543 Å, < 95.5 º)] are also observed. The strongest H-bond in the complexes is O4...H53-O6, since the angle of this interaction is 110.0 º **[37]**. As shown in Table 1, the optimized bond lengths and angles around the iron(III) ion are unaffected by the change in the type of substituent attached to the studied FQ's drugs.

The nature of the electronic transitions observed in the UV-Vis. spectra of the complexes has been studied by time-dependent DFT **[44-46]**. The lowest 30 singlet-to-singlet spin-allowed excitation states were calculated using the same functional and basis set for the optimization. The effect of solvent (DMSO) was performed using the default polarizable continuum model. The calculated d-d excitation wave lengths, energies of other excitation transitions (f > 0.002) and their assignments are taken into

consideration. The stimulated spectrum of complex **1** (Fig. S4†) shows three transitions at 445, 404, and 374 nm assigned to H(β)→L/L+1(β), H(β)→L(β) and H-4/H-5(β)→L(β) (H:HOMO; L:LUMO). The transitions at 445 nm have a ground state composed of Fe d character, whereas the excitation states are of Fe-d_{z^2} (LUMO) and Fe-$d_{x^2-y^2}$/(FQ and oxalate)-π^*orbitals (LUMO+1) forming $d \rightarrow d_{z^2}$ and $d \rightarrow d_{x^2-y^2}$/LMCT (Fig. 2) characterized to the octahedral Fe^{3+} complexes. The band at 374 nm has a LMCT character, originating from the piperazine moiety (HOMO-4) and (FQ and oxalate)-π orbitals (HOMO-5) and going to Fe d_{z^2} orbital. The TD-DFT spectrum of **2** is characterized by five transitions at 465, 420, 375, 360 and 325 nm with oscillator strengths of 0.0003, 0.0153, 0.0848, 0.0437 and 0.0101 corresponding to H(β)→L/L+1(β), H(β)→L(β), H(β)→L+1(β), H-4/H-2(β)→L(β) and H-1(β) →L+1(β). The descriptions of frontier MO's and the relocation of the electron density of complexes are nearly the same as those described in complex **1**. This is in agreement with the experimental findings, since the three complexes show similar electronic spectrum (Fig. S4†). The calculated spectrum of **3** exhibits the same transitions as observed in **1**. Comparison between the calculated and experimental spectra indicated the suitability of the applied calculation method for this size of compounds, where the experimental bands are deviated from the calculated ones by about 10 nm.

Natural bond orbital analysis and molecular electrostatic potential

Natural bond orbital (NBO) analysis **[47, 48]** and second order perturbation theory analysis of Fock Matrix provide details about the type of hybridization, nature of bonding and strength of the interactions between Fe^{3+} ion and donor sites **[49]**. The electronic arrangement of Fe in complexes **1-3** is $[Ar]4s^{0.28}3d^{6.07}4p^{0.43}5s^{0.01}5p^{0.01}$ with 6.780 valence electrons. The natural charge is 1.200 and the occupancies of Fe 3d are: $d_{xy}{}^{1.900}$ $d_{xz}{}^{1.608}$ $d_{yz}{}^{1.352}$ $d_{x^2-y^2}{}^{0.563}$ $d_{z^2}{}^{0.644}$ (**1**), $d_{xy}{}^{1.925}$ $d_{xz}{}^{1.539}$ $d_{yz}{}^{1.338}$ $d_{x^2-y^2}{}^{0.558}$ $d_{z^2}{}^{0.707}$ (**2**) and $d_{xy}{}^{1.919}$ $d_{xz}{}^{1.609}$ $d_{yz}{}^{1.356}$ $d_{x^2-y^2}{}^{0.539}$ $d_{z^2}{}^{0.644}$ (**3**). The 3d-electronic population is corresponding to the oxidation state Fe(I), not Fe(III) that is in agreement with ligand to d_{Fe} electron transfer. The strength of interactions between Fe^{3+} ion and donor sites can be estimated by the second order perturbation theory. The larger the E^2 value, the more intensive is the interaction between the electron donors and electron acceptors. For complex **1**, the E^2 values are 1.07, 0.72, 1.27, 1.33, 0.89 and 1.32 Kcal mol^{-1} for LP(3)O2→RY^*(3)Fe, LP(2)O3→RY^*(4)Fe, LP(3)O4→RY^*(2)Fe, LP(2)O5→ RY^*(3)Fe, LP(2)O6→RY^*(4)Fe and LP(3)O7→RY^*(2)Fe respectively. Similar values are observed for the other investigated complexes as tabulated in Table S1†.

Molecular electrostatic potential (MEP) map is a very useful descriptor in understanding the sites for electrophilic and nucleophilic reactions as well as H-bonding interactions **[44, 46]**. The MEP plots

(Fig. 3) of **1-3** are characterized by a positive region (blue) coming from H-atoms of FQ's and the coordinated water molecules. The negative charge region is mainly located on the oxalato O atoms and the minor contribution is coming from the carboxylate group. A zero potential area (green) is covered the remaining parts of the investigated complexes.

Thermogravimetric analysis

The thermogram of **1** exhibits four decomposition steps at 90, 233, 325 and 477 ºC. In the 1st step, only one coordinated water molecule is eliminated (mass loss: found, 3.73%; calcd. 3.53%). The 2nd stage is accompanied by a mass loss amounts to 20.74% (up to 310 ºC), which finds a parallelism with the calculated value (20.78%) responsible for loss of another water molecule and $2CO_2$. The 3rd and 4th steps bring the total mass loss up to 90.57%. Such mass loss is close to the calculated value (89.02%) expected for the formation of metallic iron as a residue. Similar, four degradation stages are observed in the TG curve of **2** at 143, 214, 331 and 405 ºC. The 1st step reveals loss of 1.5 H_2O molecules (mass loss, found, 4.73%; calcd. 5.09%). The 2nd step is assigned to removal of $0.5H_2O+2CO_2$ with a mass loss amounts to 18.25% (calcd. 18.30%). The 3rd and 4th stages are attributed to degradation of one Lf molecule giving a metallic iron as a final residue (found, 10.33%; calcd. 10.56%). The thermogram of **3** displays five decomposition steps at 102, 235, 315, 426 and 454 ºC. The 1st stage (up to 200 ºC) is responsible for desorption of $2H_2O$ (mass loss, found, 7.18%; calcd. 7.22%). The 2nd thermal event is accompanied by a mass loss amounts to 21.54%. This value goes parallel to the calculated one (21.48%) that is attributed to the elimination of $2CO_2$+1/2 F_2 molecules. The 3rd and 4th stages are corresponding to the pyrolysis of the rest of the organic part with overall mass loss amounts to 88.83% (calcd. 88.75%) leaving metallic iron as a residue.

α-Fe_2O_3 nanoparticles were prepared by heating complexes **1-3** in an electric furnace (800 ºC) under the ambient air condition before cooling to room temperature. Their XRD patterns (Fig. S5†) indicated that samples **1** and **2** are composed of single rhombohedral phase characteristic of α-Fe_2O_3 nanoparticles. All the diffraction peaks are in agreement with the reported JCPDS card no. 04-011-9585. Sample **3** is mainly α-Fe_2O_3 phase contaminated with α-FeOOH (goethite) (JCPDS card no. 00-034-1266). Fig. 4 shows FE-SEM images of the investigated α-Fe_2O_3 nanoparticles. Other FE-SEM images with a diameter of 2μm are given in Fig. S6†. As expected, the pristine nanoparticles of iron oxides bend to aggregate into large clusters because of anisotropic dipolar attraction in nanosized form of Fe_2O_3. In other words, the starting of sintering led to many grown agglomerates. The influence of the type of the coordinated FQ's has been reflected in size of the nanoparticles. The diameter of the

nanoparticles is found to be 50-120 nm (**1**), 28-54 nm (**2**) and 47-82 nm (**3**). Therefore, the thermal decomposition of lomefloxacin complex **3** gave rises to smallest iron oxide nanoparticles. EDX analysis of these particles indicates the presence of Fe and O composition in the pure as-grown iron oxide as no other peak related with any impurity has been detected (Fig.5). The sizes of the current nanoparticles are comparable to the results of several previous reports prepared iron oxide nanoparticles from the thermal decomposition conditions (13 nm-180 nm) **[8, 50]**.

Photo-degradation process

Methylene-blue (MB) is one of the generally industrial used dyes in the fields of printing, textiles, ...etc **[51]**. Its industrial effluents is the major source of harmful to the living organisms through the decrease of the dissolved oxygen capacity of water and by blocking sunlight. Severe exposure to MB led to permanent burn to the eyes of organisms, nausea and vomiting **[52]**. Therefore, the treatment of effluents containing MB is one of the challenging problems in the field of environmental chemistry. Moreover, the choice of MB in this work, as a test pollutant, to explore the catalytic performance of the synthesized nanoparticles is attributed to the high solubility in water with no possibility to volatility and gas-phase pyrolysis. Its blue solution is characterized by unique band at 665 nm, which allows easy spectrophotometrically monitoring of the degradation process **[53, 54]**. Among the different techniques used to eliminate MB, the modified Fenton reaction with various types of the synthesized catalysts **[55]** was found to be effective through the creation of highly reactive free radicals $HO^{\bullet}$ and safe by the formation of harmless chemicals such as CO_2 and H_2O. The percent of degradation depends upon the formation rate of these radicals. Heterogeneous Fenton catalyst has an advantage of working over a wider pH-range compared with the traditional one, which is limited to pH < 4. However, its disadvantage is the slower degradation rate of organic pollutants compared to the classical method. Recently, the coupling of UV irradiation with Fenton-like reagent has attracted the consideration of some working groups interested in the improvement of the degradation rate of organic pollutants such as phenol **[56]** and methylene-blue **[57]**.

To evaluate the catalytic performance of the synthesized α-Fe_2O_3 nanoparticles, the absorption spectra of the illuminated samples at various time intervals were monitored. The degradation process of MB was initiated by addition of H_2O_2 solution to the MB solution and immediately turning on the ultraviolet irradiation. For comparison, the MB degradation experiment was also done without α-Fe_2O_3 nanoparticles, but in presence of H_2O_2 and/or UV light (Fig. S7†). Fig. 6 shows the time-dependent absorption electronic spectra of MB as a function of the illumination time at 365 nm in presence of

H_2O_2/α-Fe_2O_3 nanoparticles (sample no. **2**). Similar spectra reported for sample no. **1** are giving in Fig. S8†. It can see that intensity of the characteristic band of MB at 658 nm remains nearly unchanged in the simple systems, MB+H_2O_2 and MB+UV for about 200 min. In other words, control experiments indicated that the degradation of MB is hardly proceeded in absence of catalyst (Fig. 7). The degradation efficiency [$R = 100\times((A_t-A_0)/A_0)$] of MB was determined, where A_0 and A_t are the initial absorbance and that obtained after the illumination time (t). Combined of H_2O_2 with the UV irradiation increases the percent of discolorization of MB up to about 59%. The addition of α-Fe_2O_3 nanoparticles to the MB+H_2O_2+UV system degraded about 94% (**1**), 97% (**2**) and 98 % (**3**) of MB exposed to the UV light within about 100 min. The obtained results are comparable to the previously published data used α-Fe_2O_3 nanostructured fibers as a catalyst **[58]**. The photo-catalytic degradation of MB was found to be first order reaction [$\ln(C_t/C_0)=kt$]. Its $\ln(C_t/C_0)$ plot shows a linear relationship with the illumination time (Fig. 8), where slope is the rate constant (k). The calculated rate constant for the photo-catalytic reactions was 1.26×10^{-2} (**1**), 1.89×10^{-2} (**2**) and 2.44×10^{-2} min^{-1} (**3**), while it is only about 2.00×10^{-4} (MB+UV), 1.00×10^{-4} (MB+H_2O_2) and 26×10^{-4} min^{-1} (MB+UV+H_2O_2) for blank samples. The $t_{1/2}$ value was found to be 55 (**1**), 37 (**2**) and 28 min (**3**) compared with 2.5 days (MB+UV), 5 days (MB+H_2O_2) and 4.5 hours (MB+UV+H_2O_2). It is worthy to mention that almost no degradation of MB was observed in dark, which reveals that the mechanism of the reaction is photo-degradation rather than adsorption. As shown in Fig. 7, the decrease in the particle size of the synthesized hematite nanoparticles as those coming from the thermal decomposition of complex **2,** compared with compound **1,** led to an improvement in the catalytic performance. The reactivity of iron oxide particles has been shown to greatly increase as their dimensions are reduced **[59]**. Decreasing the average particle size increases the specific surface area and thus increases the number of active surface sites. However, the presence of traces of iron oxyhydroxide in sample **3** may be the motivation for the high catalytic performance. The hydroxyl radical that comes from FeOOH may be the primary oxidant that initiate the degradation of the pollutant.

Conclusion

Reaction of ciprofloxacin, lomefloxacin and norfloxacin with $K_3[Fe(C_2O_4)_3]$ afforded complexes of the type cis-$[Fe(C_2O_4)(FQ)(H_2O)_2]$, which were characterized by several analytical and spectral tools . The experimental studies were complemented by quantum chemical calculations. Cis-isomer is found to be more stable than the trans-complex. Electronic spectra were assigned by the aid of TD-DFT calculations. Thermal decomposition of the synthesized complexes is a simple and nontoxic method for preparation of hematite (α-Fe_2O_3) nanoparticles. The purity of the hematite nanoparticles was verified

by EDX analysis. The prepared hematite nanoparticles exhibited good photo-catalytic activity in the degradation process of an industrial pollutant methylene-blue by means of Fenton-like reagent.

Experimental

Instruments

TGA was performed in nitrogen atmosphere (20 mL min^{-1}) in a platinum crucible with a heating rate of 10 ºC min^{-1} using a Shimadzu DTG-60H simultaneous DTG/TG apparatus. FT IR spectra were recorded as KBr pellets using a Jasco FTIR 460. Elemental microanalysis was performed using Elementer Vario EL III. Magnetic measurement was carried out on a Sherwood scientific magnetic balance using Gouy method **[39]**, and $Hg[Co(SCN)_4]$ was used as a calibrant. Electronic spectra were scanned on a Shimdazu Lambda 4B spectrophotometer. A digital Jenway 4310 conductivity with a cell constant of 1.02 was used for the molar conductance study. The iron oxide nanoparticle morphologies were investigated by field emission scanning electron microscope (Quanta FEG 250) attached with energy dispersive X-ray analyses for surface analysis. Hematite nanoparticles were characterized by X-ray powder diffraction (PANalytical, X'Pert PRO) operated with copper target (K_α, λ = 1.54056 Å) operated at 40 kV and 25 mA.

Synthesis

One mmol of ciprofloxacin·HCl (366 mg), lomefloxacin·HCl (386 mg) and norfloxacin (319 mg) was added to one mmol of hot aqueous solution of $K_3[Fe(C_2O_4)_3]\cdot 3H_2O$ (25 mL, 491 mg) (supplied from Sigma chemical company) and heated to reflux (1-3 h), where yellow (**1**), orange (**2**) and red (**3**) complexes were precipitated, respectively. The pH of the reaction mixture was raised by addition of ammonia solution. Lower molar conductance values (in DMF) were reported for the studied complexes compared with the reported values **[45]** for 1:1 (65-90 $\Omega^{-1}cm^2mol^{-1}$) and 1:2 (130-170 $\Omega^{-1}cm^2mol^{-1}$) electrolytes in DMF, indicating their non-ionic nature. α-Fe_2O_3 nanoparticles were prepared by heating complexes **1-3** in an electric furnace under ambient air condition before cooling to room temperature.

- Complex **1**: Color: Yellow. Elemental analysis (%): Calcd. $C_{19}H_{21}FFeN_3O_9$: C 44.73, H 4.15, N 8.24 , found C 44.68, H 4.31, N 9.04. FT IR (cm^{-1}): 3436 ν(NH), 1714 $\nu(C{=}O)_{ox}$, 1668 $\nu^{ass}(C{=}O)_{ox}$, 1628 $\nu(C{=}O)_{py}$, 1476 $\nu^{ss}(C{=}O)_{ox}$, 1386, 1271, 1181, 1106, 1034. UV-Vis. (DMF, 10^{-4}, nm): 285, 320, 335, 625. Molar Cond. (10^{-3} M, DMF, $\Omega^{-1}cm^2\ mol^{-1}$): 18.14. μ_{eff} (μ_B, 298 K): 4.86.
- Complex **2**: Color: Orange. Elemental analysis (%): Calcd. $C_{19}H_{22}F_2FeN_3O_9$: C 43.04, H 4.18, N 7.92 , found C 43.45, H 4.22, N 8.39. FT IR (cm^{-1}): 3431 ν(NH), 1714 $\nu(C{=}O)_{ox}$, 1670 $\nu^{ass}(C{=}O)_{ox}$, 1630 $\nu(C{=}O)_{py}$, 1554, $\nu^{ass}(C{=}O)$, 1523, 1459 $\nu^{ss}(C{=}O)_{ox}$, 1402, 1360 $\nu^{ass}(C{=}O)$, 1323, 1273, 1164,

1123, 1093, 1051. UV-Vis. (DMF, 10^{-4}, nm): 292, 325, 340, 625. Molar Cond. (10^{-3} M, DMF, Ω^{-1} cm^2 mol^{-1}): 9.73. μ_{eff} (μ_B, 298 K): 6.14.

– Complex **3**: Color: Red. Elemental analysis (%): Calcd. $C_{18}H_{21}FFeN_3O_9$: C 43.39, H 4.25, N 8.43 , found C 43.92, H 4.19, N 8.64. FT IR (cm^{-1}): 3442 ν(NH), 1713 $\nu(C{=}O)_{ox}$, 1665 $\nu^{ass}(C{=}O)_{ox}$, 1627 $\nu(C{=}O)_{py}$, 1548, $\nu^{ass}(C \ddot{-} O)$, 1519, 1477, 1386, 1272, 1188, 1139, 1098, 1036. UV-Vis. (DMF, 10^{-4}, nm): 285, 320, 335, 625. Molar Cond. (10^{-3} M, DMF, $\Omega^{-1}cm^2$ mol^{-1}): 10.44. μ_{eff} (μ_B, 298 K): 6.15.

Quantum chemical calculations

Ground state geometry optimization, natural bond orbital analysis and molecular electrostatic potential maps of complexes **1-3** were obtained at DFT/B3LYP/6-31G* level of theory using Gaussian03 **[60]**. The complexes were characterized as local minima through harmonic frequency analysis. Electronic transitions were calculated by TD-DFT **[44-46]**. The effect of solvent (DMSO) was performed using the default polarizable continuum model **[61]**.

Catalytic activity

The photo-catalytic degradation of MB was investigated by taking 10 mL of the dye solution (14 mg L^{-1}, pH = 5) with 0.1 mL hydrogen peroxide (35% v/v) in presence of 10 mg of nano-α-Fe_2O_3. The suspension was stirred to ensure that all the active sites of catalysts are in contact with the dye solution. Then the sample was illuminated with a UV hand lamp (365 nm) positioned perpendicular at a distance of 2 cm. The irradiation was interrupted in regular intervals to take electronic spectra on the UV-visible spectrophotometer until no more changes in the characteristic band of MB was observed.

References:

[1] K.S. Min, M.P. Suh, *J. Solid state Chem.*, 2000, **152**, 183; O. Castillo, I. Muga, A. Luque, J.M. Gutiérrez-Zorrilla, J. Sertucha, P. Román, *Polyhedron,* 1999, **18**, 1235; Y. Akhriff, J. Server-Carrió, A. Sancho, J. García-Lozano, E. Escrivá, J.V. Folgado, L. Soto, *Inorg. Chem.,* 1999, **38**, 1174.

[2] K.V. Krishnamurty, G.M. Harris, *Chem. Rev.,* 1961, **61(3)**, 213; O. Schott, J. Ferrando-Soria, A. Bentama, S. Stiriba, C. Ruiz-Pérez, M. Andruh, F. Lioret, M. Julve, *Inorg. Chim. Acta,* 2011, **376**, 358.

[3] L. Androš, M. Jurić, P. Planinić, D. Žilić, B. Rakvin, K. Molčaov, *Polyhedron*, 2010, **29**, 1291.

[4] M.J. Schmelz, T. Miyazawa, S. Mizushima, T.J. Lane, J.V. Quagliano, *Spectrochim. Acta,* 1967, **9**, 51.

[5] J.C. Blair, E.M. Jones, in: H.S. Booth (Ed.), Inorganic Synthesis, vol. 1, McGraw-Hill Book Co., New York, 1939, p. 35.

[6] A. Saritha, B. Raju, M. Ramachary, P. Raghavaiah, K.A. Hussain, *Physica B,* 2012, **407**, 4208.

[7] P.C. Junk, *J. Coord. Chem.,* 2005, **58**(4), 355.

[8] A. Saritha, B. Raju, D. Narayana Rao, A. Roychowdhury, D. Das, K.A. Hussain, *Adv. Powder Tech.,* 2015, **26**(2), 349.

[9] C.A. Parker, C.C. Hotchord, *J. Phys. Chem.,* 1959, **63**, 22; C.A. Parker, *Trans. Faraday Soc.,* 1954, **50**, 1213.

[10] W.W. Wendlandt, E.L. Simmons, *J. Inorg. Nucl. Chem.,* 1966, **28**, 2420.

[11] M. Izakovič, J. Šima, V. Brezová, *J. Photochem. Photobiol. A: Chem.,* 2004, **167**, 81.

[12] K. Sahul, L.V. Natarajan, Q. Anwaruddin, *J. Polym. Sci. Lett. Ed.,* 1977, **15**, 605.

[13] A. Abbas, I. Tajuddin, *J. Photochem.,* 1986, **35**, 87.

[14] A.S. Brar, B.S. Randhawa, *J. Solid State Chem.*, 1985, **58**, 153; *Radiochem. Radioanal. Left,* 1981, **47**, 219; *Radiochem. Radioanal. Left,* 1980, **44**, 377; A.A. Medvinskii, V.I. Poskevnev, *Zh. Strukt. Khim.,* 1974, **15**, 623; G.M. Bancroft, K.G. Dharmawardena, A.G. Maddock, *Inorg. Chem.,* 1970, **9** , 223.

[15] T.M. Muziol, G. Wrzeszcz, L. Chrzaszcz, *Polyhedron,* 2011, **30**, 169. R. Prasad, Sulaxna, A. Kumar, *J. Therm. Anal. Calorim.,* 2005, **81**, 441.

[16] P.K. Gallagher, C.R. Kurkjian, *Inorg. Chem.,* 1965, **5**, 214; D. Broadbent, D. Dollimore, J. Dollimore, *J. Chem. Soc. A,* 1967, 451; W.W. Wendlandt, T.D. George, *J. Inorg. Nucl. Chem.,* 1961, **21**, 69.

[17] O. Paulsen, *Drugs Today,* 1987, **23**, 269.

[18] V.T. Andriole, *Clin. Infect. Dis.,* 2005, **41**, S113; D.C. Hooper, E. Rubinstein (Eds.), Quinolone Antimicrobial Agents, third Ed., ASM Press, Washington, DC, 2003; D. C. Hooper, J. S. Wolfson, E.Y. Ng, M. N. Swartz, *Am. J. Med.* (Suppl. 4A), 1987, **82**, 12.

[19] D.E. King, R. Malone, S.H. Lilley, *Am. Fam. Physician,* 2000, **61**, 2741.

[20] H.K. Mayer, J.A. Ellal, *Am. J. Med.,* 1999, **92**, 58S; G.S. Ogawa, R. Hyndiuk, *Int. Ophthalmol. Clin.,* 1993, **33**, 59.

[21] I. Turel, *Coord. Chem. Rev.,* 2002, **232**(1-2), 27.

[22] L. Fratini, E.E.S. Schapoval, *Int. J. Pharm.,* 1996, **127**, 279.

[23] D.S. Lee, H. Han, K. Kim, W.B. Park, J.K. CHO, J.H. Kim, *J. Pharm. Biomed. Anal.,* 1994, **12**(2), 157; J. Al-Mustafa, B. Tashtoush, *J. Coord. Chem.,* 2003, **56**(2), 113.

[24] P.B. Issopoulos, *Analyst,* 1989, **114**, 627.

[25] D.L. Ross, C.M. Riley, *Int. J. Pharmaceutics,* 1992, **87**, 203.

[26] F. Gao, P. Yang, J. Xie, H. Wang, *J. Inorg. Biochem.,* 1995, **60**, 61.

[27] S.A. Sadeek, *J. Mol. Struct.,* 2005, **753**, 1.

[28] S.C. Wallis, L.R. Gahan, B.G. Charles, T.W. Hambely, *Polyhedron,* 1995, **14**(20-21), 2835.

[29] G. Psomas, *J. Inorg. Biochem.,* 2008, **102**, 1798.

[30] H.F. Abdel-Halim, G.G. Mohamed, M.M.I. El-Dessouky, W.H. Mahmoud, *Spectrochim. Acta,* 2011, **82**, 8.

[31] L.C. Yu, Z.L. Tang, P.G. Yi, S.L. Liu, *J. Coord. Chem.,* 2009, **62**(6), 894.

[32] J.L.R. Costa, G.S. Marchetti, M.C. Rangel, *Catal Today,* 2002, **77**, 205; C. Huang, H. Zhang, Z. Sun, Y. Zhao, S. Chen, R. Tao, Z. Liu, *J. Colloid Interface Sci.,* 2011, **364**, 298.

[33] J. Zhang, S. Rama, R.S. Srivastava, R.D.K. Misra, *Acta Biomater,* 2008, **4**, 40; S. Ghoshal, A. A.M. Ansar, S.O. Raja, A. Jana, N.R. Bandyopadhyay, A.K. Dasgupta, M. Ray, *Nanoscale Res. Lett.,* 2011, **6**, 540.

[34] Z. Medarova, W. Pharm, C. Farrar, V. Petkova, A. Moore, *Nat. Med.,* 2006, **13**(3), 372.

[35] A.H. Lu, E.L. Salabas, F. Schüth, *Angew Chem. Int. Ed.,* 2007, **46**, 1222.

[36] F. Gao, P. Yang, J. Xie, H. Wang, *J. Inorg. Biochem.,* 1995, **60**, 61.

[37] A.M. Mansour, O.R. Shehab, *Spectrochimica Acta Part A,* 2014, **128**, 263.

[38] D.K. Saha, D. Deobagkar, U. Sandbhor, K. Shirisha, C.E. Anson, S. Padhye, A.K. Powell, *Bioorg. Med. Chem. Lett.,* 2004, **14**, 3027.

[39] N.T. Abdel-Ghani, M.F. Abo El-Ghar, A.M. Mansour, *Spectrochim. Acta A,* 2013, **104**, 134.

[40] I. Turel, I. Leban, N. Bukovec, *J. Inorg. Biochem.,* 1994, **56**, 273.

[41] A.M. Mansour, R.R. Mohamed, *RSC Adv.,* 2015, **5**, 5415.

[42] A. Bentama, O. Schott, J. Ferrando-Soria, S. Stiriba, C. Ruiz-Pérez, M. Julve, J. Pasán, *Inorg. Chim. Acta,* 2012, **389**, 52; X. Chen, L. Liu, J. Ma, L. Yi, P. Cheng, D. Liao, S. Yan, Z. Jiang, *J. Mol. Struct.,* 2005, **750**, 94.

[43] M. Massacesi, G. Ponticelli, *Spectrochim.,* 1981, **37**A(12), 1035.

[44] A.M. Mansour, *Polyhedron,* 2014, **78**, 10.

[45] A.M. Mansour, *Dalton Trans.,* 2014, **43**, 15950.

[46] O.R. Shehab, A.M. Mansour, *J. Mol. Struct.,* 2013, **1047**, 121.

[47] A.E. Reed, L.A. Curtiuss, F. Weinhold, *Chem. Rev.,* 1988, **88**, 899.

[48] N.T. Abdel-Ghani, A.M. Mansour, *Inorg. Chim. Acta,* 2011, **373**, 249.

[49] A.M. Mansour, *Inorg. Chim. Acta,* 2013, **408**, 186.

[50] P. Guardia, J. Pérez-Juste, A. Labarta, X. Batlle, L.M. Marza, *Chem. Commun.,* 2010, **46**, 6108.

[51] B. Zargar, H. Parham, M. Rezazade, *J. Chin. Chem. Soc.-Taip.,* 2011, **58**, 694.

[52] M. Rafatullaha, O. Sulaimana, R. Hashim, *J. Hazard. Mater.,* 2010, **177**, 70.

[53] M. Amini, B. Pourbadiei, T.P.A. Ruberu, L.K. Woo, *New J. Chem.,* 2014, **38**, 1250.

[54] I. Ursachi, A. Stancu, A. Vasile, *J. Colloid Interface Sci.,* 2012, **377**, 184.

[55] P.V. Nidheesh, *RSC Adv.,* 2015, **5**, 40552.

[56] M.A. Andrade, R.J. Carmona, A.S. Mestre, J. Matos, A.P. Carvalho, C.O. Ania, *Carbon*, 2014, **76**, 183; G. Thennarasu, A. Sivasamy, *Powder Technology,* 2013, **250**, 1.

[57] S. Chin, E. Park, M. Kim, J. Jurng, *Powder Technology,* 2010, **201**, 171; E.M. Seftel, M. Niarchos, Ch. Mitropoulos, M. Mertens, E.F. Vansant, P. Cool, *Catalysis Today,* 2015, **252**, 120.

[58] Y. Liu, Y. Li, H. Yu, Z. Lv. Y. Yu, S. Zhan, X. Yang, *J. Sol-Gel Sci. Technol.,* 2011, **58**, 716.

[59] E.O. Kajander, N. Ciftcioglu, *Proc. Natl. Acad. Sci. U.S.A.,* 1998, **95**, 8274.

[60] M.J. Frisch, G.W. Trucks, H.B. Schlegel, G.E. Scuseria, M.A. Robb, J.R. Cheeseman, V.G. Zakrzewski, J.A. Montgomery, R.E. Stratmann, J.C. Burant, S. Dapprich, J.M. Millam, A.D. Daniels, K.N. Kudin, M.C. Strain, O. Farkas, J. Tomasi, V. Barone, M. Cossi, R. Cammi, B. Mennucci, C. Pomelli, C. Adamo, S. Clifford, J. Ochterski, G.A. Petersson, P.Y. Ayala, Q. Cui, K. Morokuma, D.K. Malick, A.D. Rabuck, K. Raghavachari, J.B. Foresman, J. Cioslowski, J.V. Ortiz, A.G. Baboul, B.B. Stefanov, G. Liu, A. Liashenko, P. Piskorz, I. Komaromi, R. Gomperts, R.L. Martin, D.J. Fox, T. Keith, M.A. Al-Laham, C.Y. Peng, A. Nanayakkara, C. Gonzalez, M. Challacombe, P.M.W. Gill, B. G. Johnson, W. Chen, M.W. Wong, J.L. Andres, M. Head-Gordon, E.S. Replogle, J.A. Pople, GAUSSIAN 03 (Revision A.9), Gaussian, Inc., Pittsburgh, 2003.

[61] N.T. Abdel-Ghani, A.M. Mansour, *Spectrochim. Acta Part A,* 2012, **91**, 272.

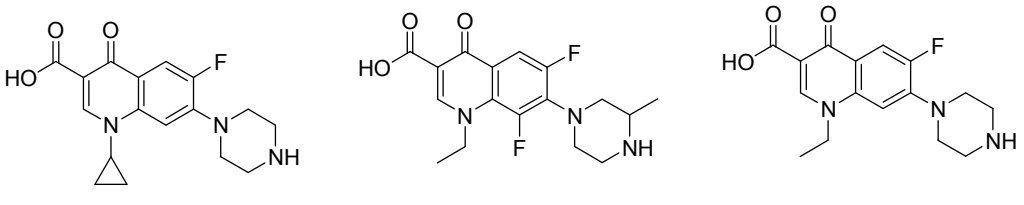

(a)

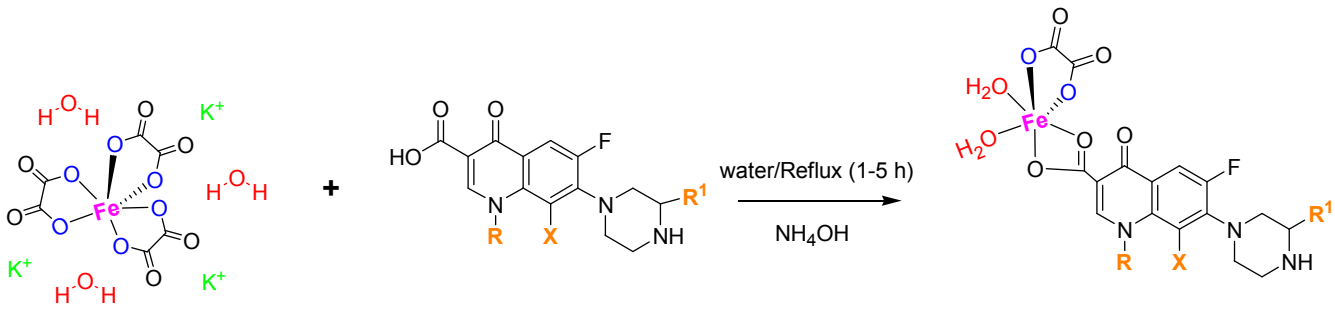

R = Cyclopropyl, X = R^1 = H (Ciprofloxacin) (**1**)
R = Ethyl, X = F, R^1 = methyl (Lomefloxacin) (**2**)
R= Ethyl, X = R^1 = H (Norfloxacin) (**3**)

(b)

Scheme 1: a) Structures of the investigated fluoroquinolones (FQ's) and **b)** Synthesis of $[Fe(C_2O_4)(FQ)(H_2O)_2]$ complexes.

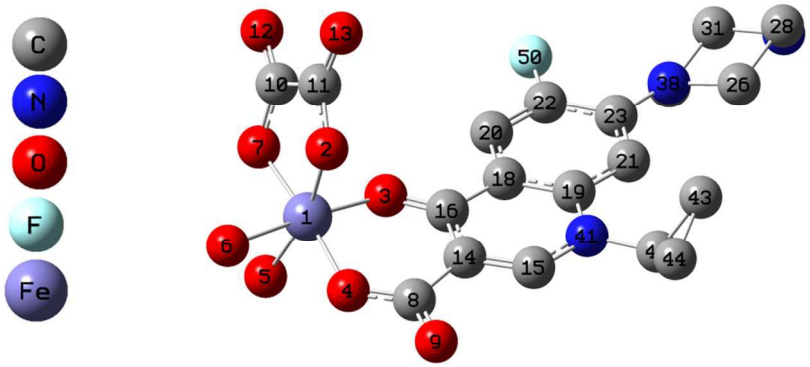

a)

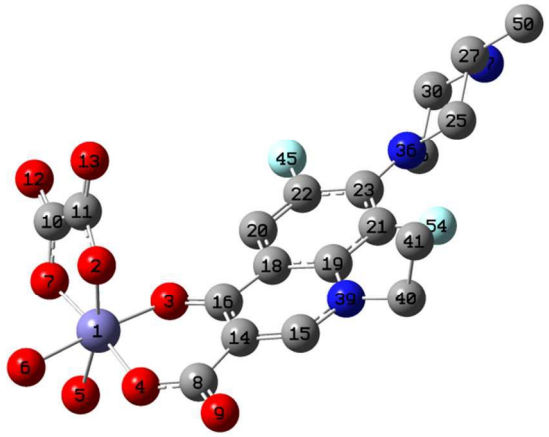

b)

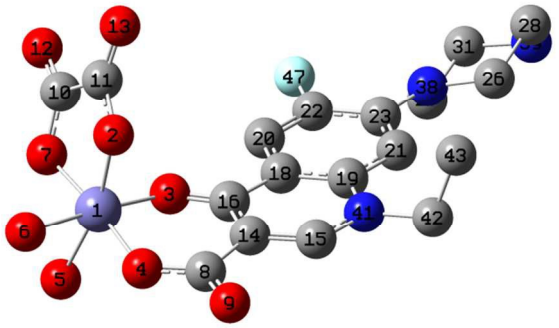

c)

Fig. 1: Local minimum structures of complexes a) **1**, b) **2** and c) **3** obtained at DFT/B3LYP/6-31G(d) level of theory.

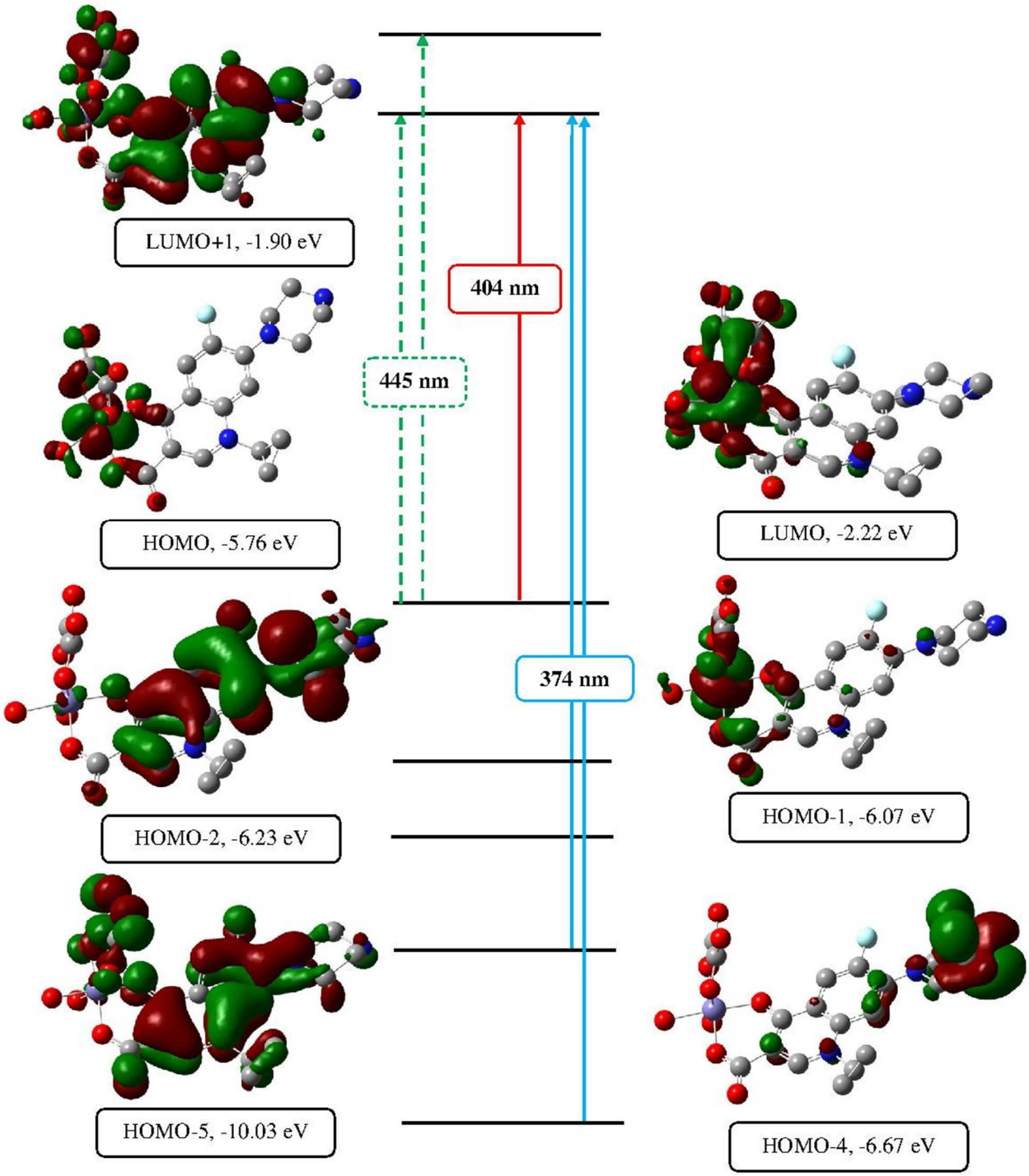

Fig. 2: Theoretical electronic absorption transitions of complex **1** in DMSO.

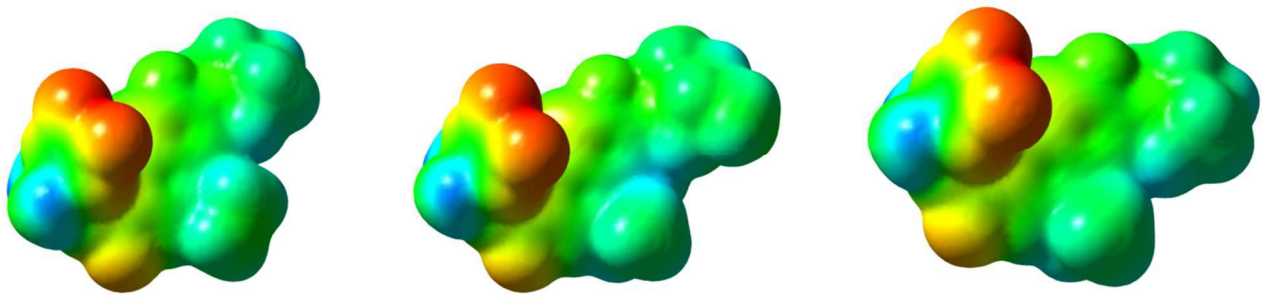

1 **2** **3**

Fig. 3: Molecular electrostatic potential map for complexes a) **1**, b) **2** and c) **3**. The electron density isosurface is 0.004 a.u. Different values of the electrostatic potential are represented by different colors: red represents the regions of the most electro negative potential, blue represents regions of most positive electrostatic potential and green represents regions of zero potential. Potential increases in the following order: red < orange < yellow < green < blue.

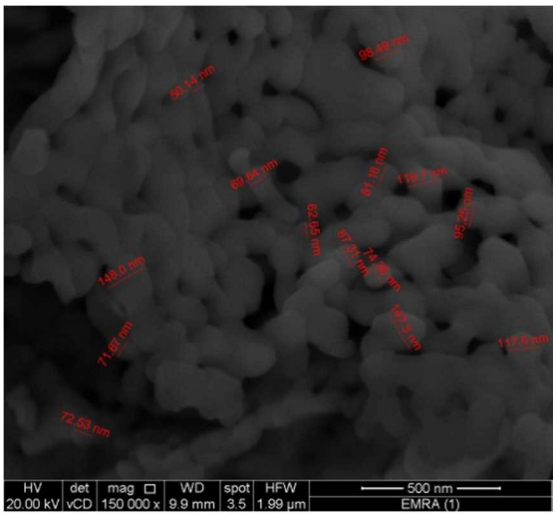

a)

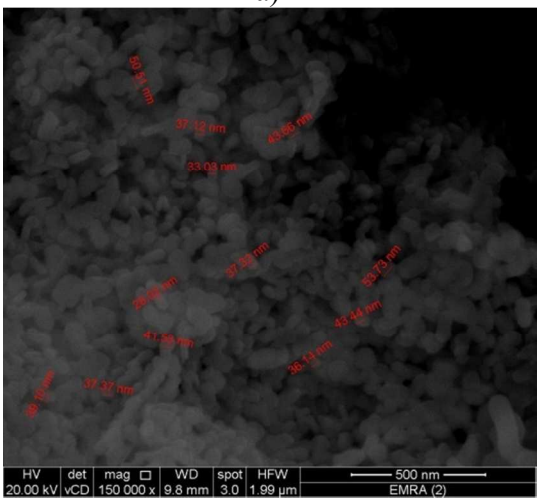

b)

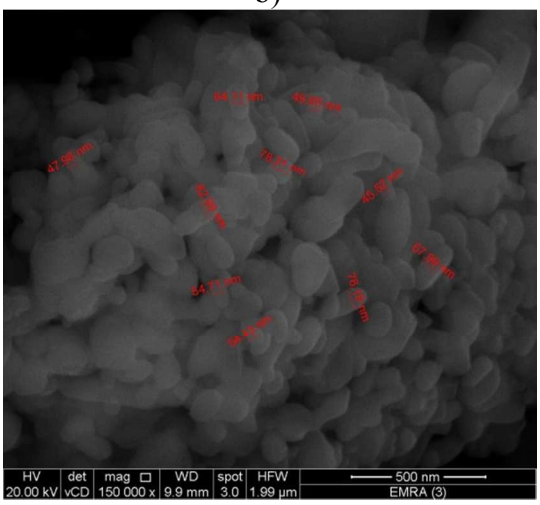

c)

Fig. 4: FE-SEM images of α-Fe_2O_3 nanoparticles obtained from thermal decomposition of a) **1**, b) **2** and c) **3**.

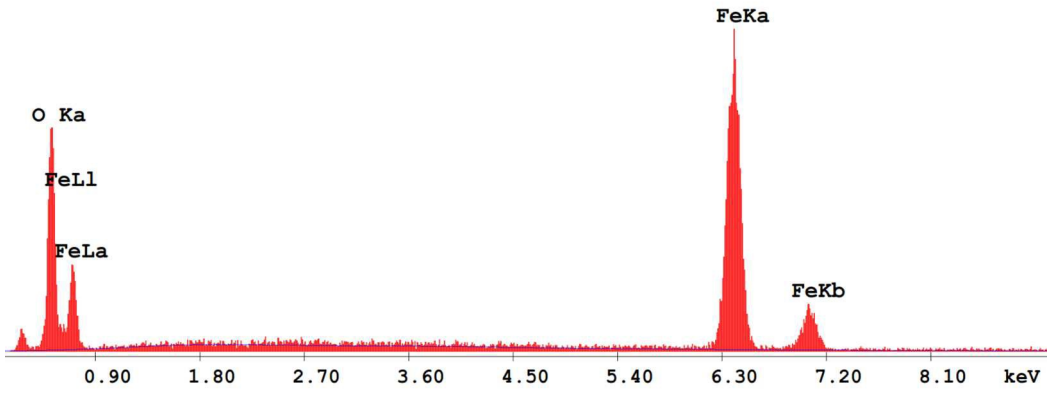

a)

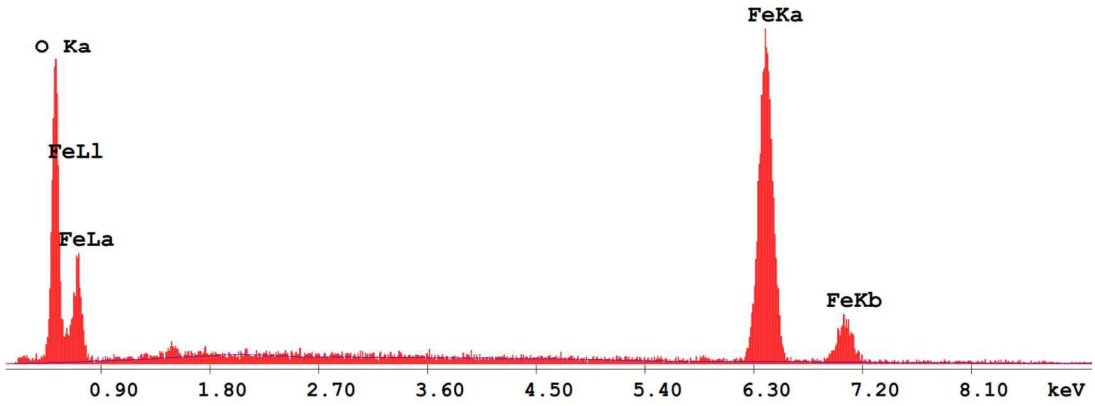

b)

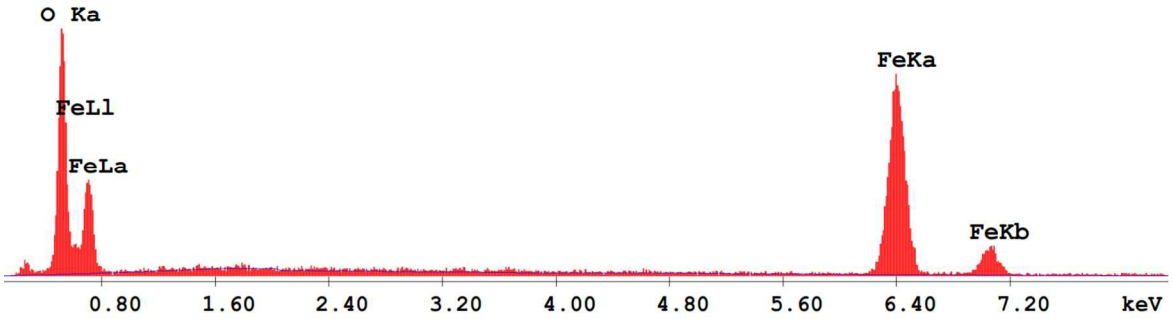

c)

Fig. 5: EDX analysis of α-Fe_2O_3 nanoparticles obtained from thermal decomposition of a) **1**, b) **2** and c) **3**.

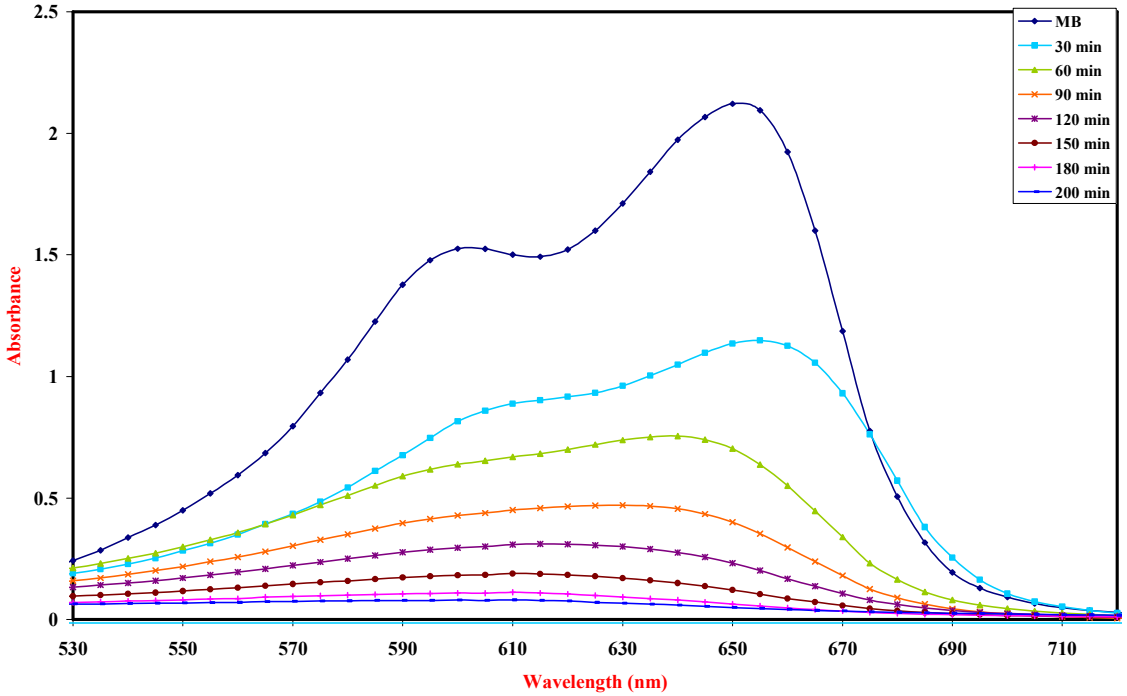

Fig. 6: Time-dependent UV-vis. absorption spectra for the photocatalytic degradation of MB with α-Fe_2O_3 (**2**) [10 mL dye (14 mg L^{-1}), 0.1 mL H_2O_2 (35%), 10 mg α-Fe_2O_3, λ = 365 nm].

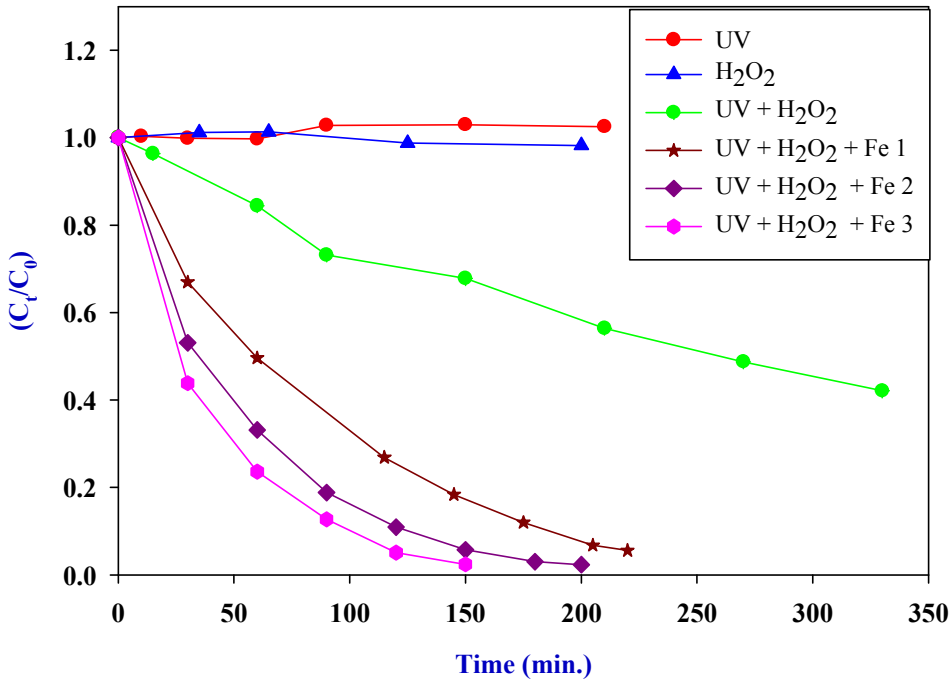

Fig. 7: Ultraviolet light photo-degradation of MB under different conditions.

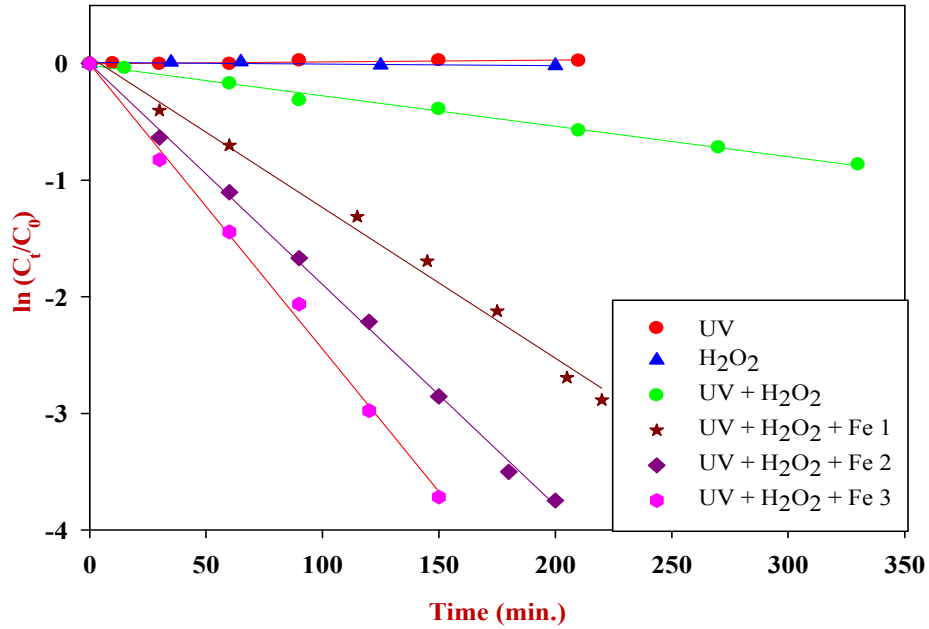

Fig. 8: Linear plots of $\ln(C_t/C_0)$ vs. time for the decolorization of MB under different conditions.

Table 1: Selected bond lengths (Å) and angles (º) for complexes **1-3** calculated by DFT/B3LYP/ 6-31G(d) method

Bond lengths (Å)				**Angles (º)**			
	1	**2**	**3**		**1**	**2**	**3**
FeO2	1.840	1.840	1.840	O2FeO3	93.6	93.4	93.6
FeO3	1.893	1.895	1.893	O2FeO4	97.1	97.1	97.1
FeO4	1.877	1.876	1.877	O2FeO5	165.9	166.1	165.9
FeO5	2.033	2.033	2.033	O2FeO6	87.5	87.7	87.5
FeO6	2.026	2.024	2.026	O2FeO7	85.8	85.8	85.8
FeO7	1.882	1.881	1.882	O3FeO4	96.1	96.1	96.1
				O3FeO6	175.7	175.8	175.7
				O4FeO7	174.5	174.5	174.5
				O4FeO6	79.6	79.7	79.6
				O6FeO7	95.9	95.8	95.9